

Compositional bowing of band energies and their deformation potentials in strained InGaAs ternary alloys: a first-principles study

Petr A. Khomyakov,* Mathieu Luisier, and Andreas Schenk

Integrated Systems Laboratory, Department of Information Technology and Electrical Engineering, ETH Zurich, Gloriastrasse 35, 8092 Zurich, Switzerland

(Dated: August 26, 2015)

Using first-principles calculations, we show that the conduction and valence band energies and their deformation potentials exhibit a non-negligible compositional bowing in strained ternary semiconductor alloys such as InGaAs. The electronic structure of these compounds has been calculated within the framework of local density approximation and hybrid functional approach for large cubic supercells and special quasi-random structures, which represent two kinds of model structures for random alloys. We find that the predicted bowing effect for the band energy deformation potentials is rather insensitive to the choice of the functional and alloy structural model. The direction of bowing is determined by In cations that give a stronger contribution to the formation of the $\text{In}_x\text{Ga}_{1-x}\text{As}$ valence band states with $x \gtrsim 0.5$, compared to Ga cations.

III-V semiconductor compounds are considered for the integration with Si-based microelectronics to take advantage of their high charge carrier mobility.¹ This has been driving basic and applied research on various aspects of the III-V semiconductor materials as well as on the device design.¹⁻³ One field of extensive research is to understand how the electronic properties of the III-V compounds are altered by stress that is externally applied to tailor characteristics of semiconductor nanodevices.^{1,4,5}

Though III-V compounds such as InGaAs are important material systems, measuring their electronic properties is a formidable challenge, partly due to their narrow gap. As a consequence, rather scattered experimental data have been reported so far, especially for the X and L conduction band valleys,⁶ suggesting that reliable theoretical studies are needed. Knowing deformation potentials of the band gap, valence band splitting and higher energies of conduction band minima is of particular interest for opto- and nanoelectronics.^{5,6} So far, the bulk of the theoretical work has been done within the framework of the empirical pseudopotential method combined with virtual crystal approximation (VCA).^{7,8} These methods require adjustable parameters fitted to the existing experimental data. Nowadays, the state-of-the-art first-principles methods allow for large-scale atomistic, parameter-free calculations of the properties of disordered materials⁹ as well as parameter-free VCA calculations.¹⁰ A recent first-principles study has predicted a strong compositional bowing of deformation potentials in group III-nitride semiconductor compounds,¹¹ not supporting an assumption of a negligible bowing.¹² There has been no systematic atomistic study of the compositional bowing effect in the strained InGaAs ternary alloy, which is a channel material of high relevance for modern types of field-effect transistors.¹⁻³

In this Letter, we have done first-principles calculations of the band structure parameters for strained $\text{In}_x\text{Ga}_{1-x}\text{As}$ compounds as a function of alloy composition, x . These ternary alloys have been modeled using 32-atom special quasi-random structures (SQSs),¹³⁻¹⁵ and 216-atom cubic supercell (SC) structures with In and Ga

atoms randomly distributed over the lattice sites. The binary alloys (GaAs and InAs) are first treated with a primitive 2-atom cell for highly converged reference calculations. The supercell approach is then adopted for correlated calculations of the physical properties of the binary InAs and GaAs, and ternary $\text{In}_x\text{Ga}_{1-x}\text{As}$ alloys with $x = 0.25, 0.50$, and 0.75 . Using density functional theory (DFT) approach, we have obtained the compositional dependence for the hydrostatic deformation potentials of the band gap and higher conduction band energies at the L and X valley minima as well as two shear deformation potentials for the valence band splitting at the Γ point. These calculations have been done for several random configurations of 216-atom supercell alloy structures to compute configurational averages of the physical quantities. We interpolate the DFT-derived compositional dependence of a physical quantity, Q , as

$$Q(x) = xQ(1) + (1-x)Q(0) - b_w x(1-x), \quad (1)$$

where b_w is a bowing parameter, and $Q(0)$, $Q(x)$ and $Q(1)$ correspond to GaAs, $\text{In}_x\text{Ga}_{1-x}\text{As}$ and InAs, respectively. The bowing is assumed to be upward (downward) for $b_w < 0$ ($b_w > 0$). Our results predict a sizable compositional bowing of band energies and their deformation potentials ($b_w \neq 0$), contrary to the widely used Vegard law ($b_w = 0$).^{6,12} The bowing effect of the deformation potentials is attributed to a stronger contribution of the p -orbitals of In cations to the formation of the alloy valence band states compared to that of Ga for $x \sim 0.5$.

We perform the DFT calculations within the framework of the plane-wave pseudopotential approach combined with the projector augmented wave (PAW) formalism¹⁶ as implemented in the VASP code.^{17,18} Local density approximation (LDA)¹⁹ and hybrid functional approach (HSE06)²⁰ are adopted for the DFT calculations. The Brillouin zone (BZ) is sampled with a $12 \times 12 \times 12$, $4 \times 4 \times 2$, and $2 \times 2 \times 2$ k-point grid for the 2-atom primitive cell, 32-atom SQS, and 216-atom cubic supercell structures, respectively. The k-meshes are chosen to include the Γ , X and L points in the BZ. A kinetic energy cut-off of 400 eV is used for total energy calculations to converge

the total energy to 10^{-6} eV and interatomic forces to $\sim 10^{-3}$ eV/Å at least. Our supercell calculations suggest that Vegard's law is a good approximation for the lattice constant of the fully optimized $\text{In}_x\text{Ga}_{1-x}\text{As}$ structures, i.e., $a(x) \approx x a_{\text{InAs}} + (1-x) a_{\text{GaAs}}$, where $a_{\text{InAs}}=6.104$ Å (6.032 Å) and $a_{\text{GaAs}}=5.677$ Å (5.611 Å) are obtained with the HSE (LDA) functional. For the sake of comparison, we have also done alloy calculations using a modern version of the virtual crystal approximation (VCA) based on the DFT approach.¹⁰ This DFT-VCA scheme predicts, however, an anomalous compositional bowing of the lattice constant and band energies in contradiction with experiment and supercell calculations.²¹ Additional computational details can be found in the supplementary material (SM).²²

Using the lattice parameters, $a(x)$, we have calculated the electronic structure of the InGaAs ternary alloys to obtain the relevant band energies at the Γ , L and X valley minima as a function of alloy composition as shown in Fig. 1. The figure reveals a non-negligible downward bowing for the band-gap energy ($E_g = E_\Gamma$), suggesting that the Vegard law is a rough approximation for the compositional dependence of the InGaAs band gap. The hybrid functional calculations give a bowing parameter of ~ 0.55 eV in a good agreement with that of 0.43 and 0.48 eV found in experiment at $T = 0$ and 300 K, respectively. The overall accuracy of the calculated band gap compared to the experimental data is in the range of 4-14% depending on the alloy composition and temperature, and whether the spin-orbit interaction is taken into account or not. Hereafter, we neglect the spin-orbit interaction, assuming that it does not significantly affect the compositional bowing of band energies and their deformation potentials.²³ This is a plausible assumption since the spin-orbit splitting, Δ_{so} , of top valence bands at the Γ -point depends weakly on the InGaAs alloy composition as given by $\Delta_{\text{so}}(x)$, which is 0.36 and 0.38 eV for GaAs ($x = 0$) and InAs ($x = 1$), respectively.

To verify that the compositional bowing does not depend on a particular choice of the alloy structural model that accounts for configurational disorder, we explicitly show in Fig. 1 that the 32-atom SQS and 216-atom cubic supercell models give consistently similar values for the band gap. The band gap calculated for the 32-atom SQSs exhibits a certain alloy broadening for the $\text{In}_x\text{Ga}_{1-x}\text{As}$ alloy with $x = 0.5$ because the three top valence bands are split by alloy disorder. Increasing the supercell size to 216 atoms reduces this effect as seen in Fig. 1. This suggests that some physical quantities of the ternary alloys may suffer from a finite-size effect as a result of treating alloy disorder with relatively-small model structures. It also means that actual alloy broadening of the band gap is likely to be rather small in the limit of an infinitely (or sufficiently) large ternary alloy structure, but it may manifest itself in alloy nanostructures.

Figure 1 also shows how the conduction band energies of the InGaAs alloys at the L and X valley minima depend on alloy composition. We find that the conduction

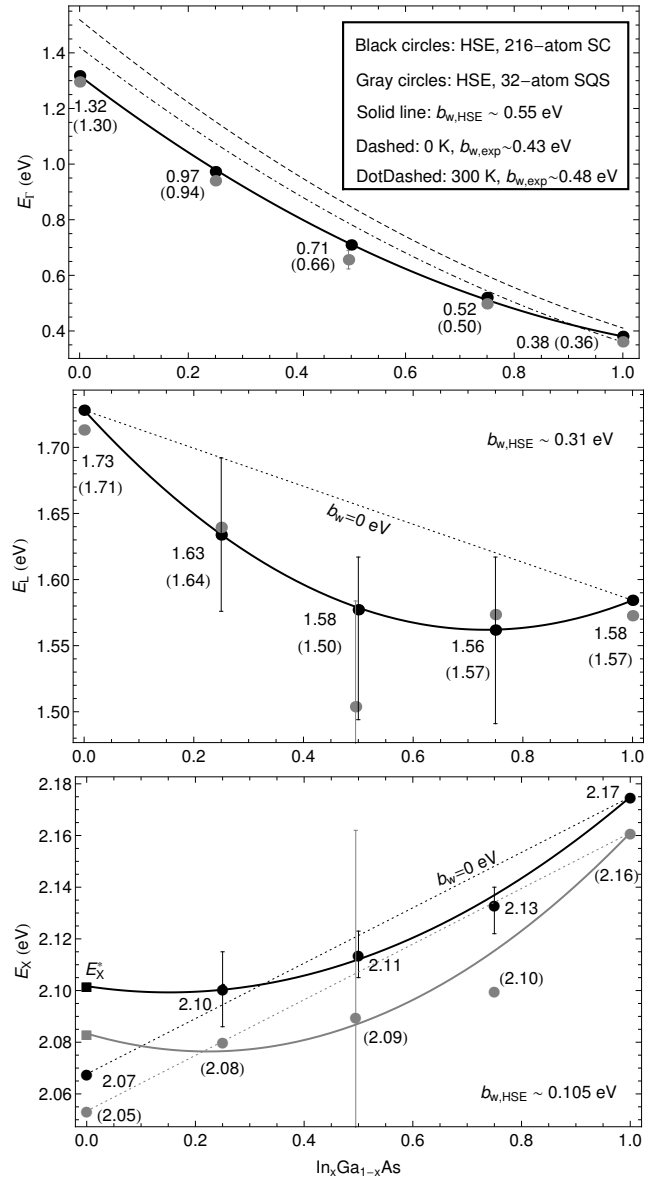


FIG. 1. Compositional dependence of the conduction band energies E_Γ , E_L and E_X averaged over the one Γ , four L , and three X valley energies, respectively. The HSE-calculated energies (black and gray filled circles) are defined with respect to the valence band energy averaged over top three valence bands (split by alloy disorder) at the Γ point. The experimental data are taken from Refs. 6 and 24. Filled squares correspond to $E_{X,\text{GaAs}}^*$, which is the conduction band energy of GaAs exactly at the X point of the BZ. All the lines are given by Eq. (1). The "error" bars are given by a disorder-induced energy splitting at the effective L (X) point of the virtual fcc crystal BZ of InGaAs. Note that these bars are not related to an error, but rather quantify a real effect of alloy broadening. The latter are not a measure for an uncertainty due to different atom arrangements, which is within RT of 25 meV only.

band energy, E_L , at the L -point exhibits strong compositional bowing, suggesting that Vegard's law is not applicable for this band parameter. The conduction band energy, E_X , at the X valley minimum has a nonlinear behavior with respect to alloy composition as well, see Fig. 1. The figure suggests that the alloy broadening of these energies is more significant compared to that of the band gap. Unfortunately, there are no reliable experimental data for the higher conduction band energies of the $\text{In}_x\text{Ga}_{1-x}\text{As}$ alloys with $x > 0$ so that we provide a parameter-free prediction of their values.

The higher energies are more prone to alloy disorder due to a different character of the electronic states at the L and X valley minima compared to that of the electronic state at the Γ point. The latter is an isotropic, s -like state that should be rather insensitive to some structural anisotropy induced by disorder in the InGaAs alloy. The electronic states at the four L and three X valleys of the BZ are anisotropic due to their mixed sp -like character that makes them more sensitive to alloy disorder. In the supercell calculations, we observe it as a four (three)-fold degeneracy lift, i.e., energy level splitting, at the effective $L(X)$ valley in the virtual face-centered cubic (fcc) crystal BZ, which can be defined for the InGaAs alloys in virtual crystal approximation. We compute the actual conduction band energies shown in Fig. 1 as an average of the corresponding four (three) energies at the effective $L(X)$ valley. The alloy broadening of the band energies is proportional to the disorder-induced energy level splitting, see Fig. 1. Though this splitting can be sizeable, the averaged conduction band energies are insensitive to configurational disorder with some exception for $x \sim 0.5$. That is demonstrated by using two different structural models of random alloys (the SQS and cubic supercells) that give similar averaged energies as shown in Fig. 1. Thus, we provide a reliable prediction for the average band structure of InGaAs even though alloy broadening might be overestimated because of the finite-size effect.

We now describe how the conduction band energies are affected by hydrostatic strain. The corresponding deformation potential, a_C , is given by $E_C(\epsilon) = E_C(0) + 3a_C\epsilon$ with $C = \Gamma, L$ and X , where $\epsilon = \epsilon_{xx} = \epsilon_{yy} = \epsilon_{zz} \neq 0$ are the only non-zero elements of the strain tensor.^{22,23} A larger absolute value of the deformation potential means a stronger strain influence on the alloy band structure, and the sign of a_C suggests a qualitative behavior of the band energies with respect to the compressive ($\epsilon < 0$) and tensile ($\epsilon > 0$) strain conditions. Using the LDA and HSE functionals, we have calculated the band-gap hydrostatic deformation potential, a_Γ , for the 216-atom cubic supercell structures of the $\text{In}_x\text{Ga}_{1-x}\text{As}$ ternary alloys as a function of alloy composition as given in Fig. 2. The LDA (HSE) calculations agree (very well) with the experimental data for the GaAs and InAs binary alloys. For the InGaAs ternary alloys, a non-negligible *upward* bowing is predicted for a_Γ , see Fig. 2. The 32-atom SQS model shows a similar upward behavior for the compositional bowing of a_Γ , proving that we have done configu-

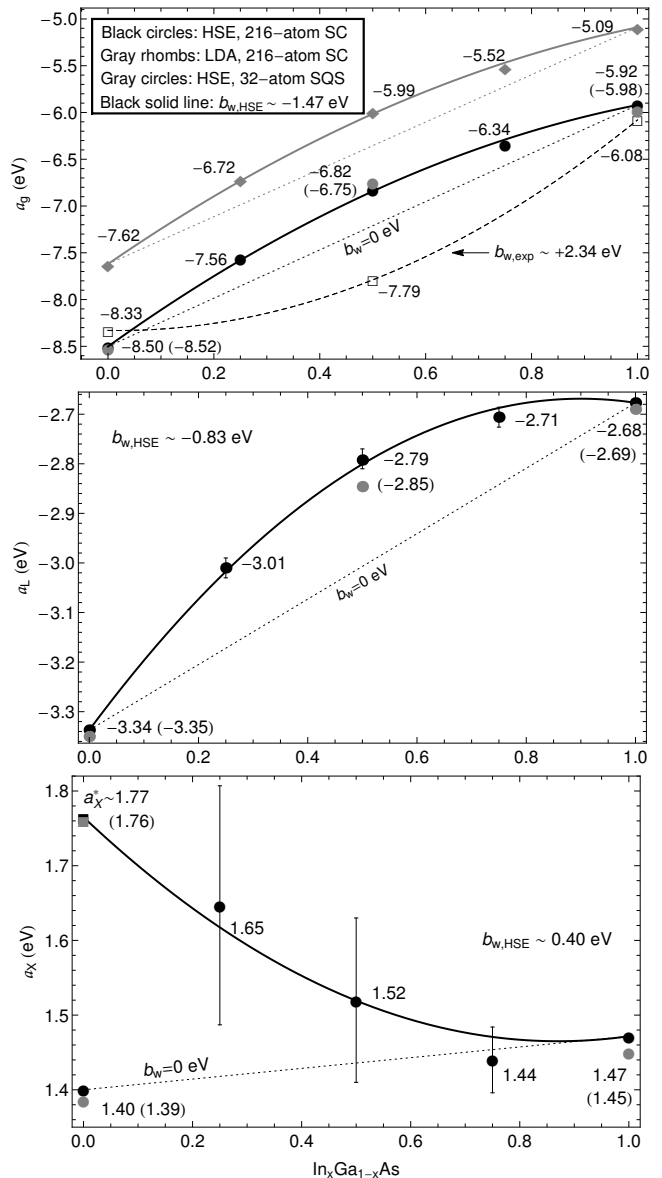


FIG. 2. Compositional dependence of the hydrostatic deformation potentials (a_Γ , a_L and a_X) of the conduction band energies that are defined as $a_C = [a_C(\epsilon = 0+) + a_C(\epsilon = 0-)]/2$ with $C = \Gamma, L$ and X , where $a_C(\epsilon = 0+)$ and $a_C(\epsilon = 0-)$ are calculated with the HSE (filled circles and squares) and LDA (filled gray rhombs) functionals for the tensile and compressive strain conditions, respectively. Filled squares correspond to the deformation potential, a_X^* , for the conduction band energy of GaAs exactly at the X point of the BZ. The "error" bars correspond to alloy disorder-induced anisotropy quantified as $|a_C(\epsilon = 0+) - a_C(\epsilon = 0-)|$. The open squares are related to the experimental data.⁶ All the lines are given by Eq. (1).

rational averaging of this physical parameter properly.

Having a good agreement with experiment for the two binary alloys (GaAs and InAs) suggests that the HSE calculations should allow for reliable prediction of hy-

drostatic deformation potentials for the corresponding ternary alloys. Though three experimental data points for the $\text{In}_x\text{Ga}_{1-x}\text{As}$ alloys with $x = 0.0, 0.5,$ and 1.0 (Fig. 2) seem to suggest a *downward* compositional bowing of the band-gap hydrostatic deformation potential, we would like to point out that these data are taken from three uncorrelated sources.⁶ Another explanation is that determining a_g from row experimental data requires separating the hydrostatic and shear strain effects on the band gap. This procedure relies on the knowledge of elastic constants for InGaAs, which are usually estimated from Vegard's law. However, we have found that the elastic constant compositional dependence of the InGaAs compounds deviates from the Vegard law as discussed in SM,²² and this might be a reason for the discrepancy.

Besides the band-gap energy of the InGaAs compounds, the hydrostatic strain affects the higher energies at the L and X valley minima. The corresponding deformation potentials are given as a function of alloy composition in Fig. 2. One can clearly see that there exists a strong upward (downward) bowing of the hydrostatic deformation potential, a_L (a_X), for the conduction band energy exactly at the L (X) point. For the X valley minimum, $a_X(x)$ exhibits a non-monotonic behavior, reaching its maximum at $x < 0.25$. We find that the deformation potential, a_L , exhibits a modest alloy-induced anisotropy (proportional to alloy broadening) given with "error" bars in Fig. 2. That is confirmed by the HSE calculations done for the 32-atom SQS and 216-atom cubic supercell structures that represent two different models for configurational disorder in the InGaAs ternary alloys. On the contrary, the hydrostatic deformation potential, a_X , suffers from a significantly larger alloy broadening than a_L . That is mainly due to strain-induced chemical hybridization of the electronic states at the effective X -point of the supercell (unfolded) BZ.

The band structure of the $\text{In}_x\text{Ga}_{1-x}\text{As}$ ternary alloy can also be modified by two shear deformations (I) $\epsilon = \epsilon_{xx} - \epsilon_{yy}$, $\epsilon_{yy} = -\epsilon_{xx} \neq 0$ and $\epsilon_{zz} = 0$, and (II) $\epsilon = \epsilon_{xy} = \epsilon_{yx} \neq 0$.^{12,23} One of three top valence bands at the Γ point is not altered by shear strain whereas two other valence bands are split symmetrically by the strain. The corresponding splitting energy is given as $\Delta E_v = D|\epsilon|$ in the linear approximation, which we find to be valid up to $\epsilon \sim 0.01$ at least. We define two shear deformation potentials as $D_{\text{I}} = 3b$ and $D_{\text{II}} = 2 \times 3^{1/2}d$, where b and d correspond to the shear strain I and II according to $k \cdot p$ model conventions.^{4,25} The microscopic parameters obtained from our DFT calculations can then be directly employed for this phenomenological model. The shear strain affects the band gap by decreasing it to $E_g(0) - |\Delta E_v|/2$ unlike the hydrostatic strain that can enlarge or narrow the gap, depending on the sign of ϵ . The electronic states at the Γ (X , L) valley are unaffected (somewhat affected) by shear strain, see SM.²²

Figure 3 shows how the shear deformation potentials (b and d) depend on alloy composition. One can see that

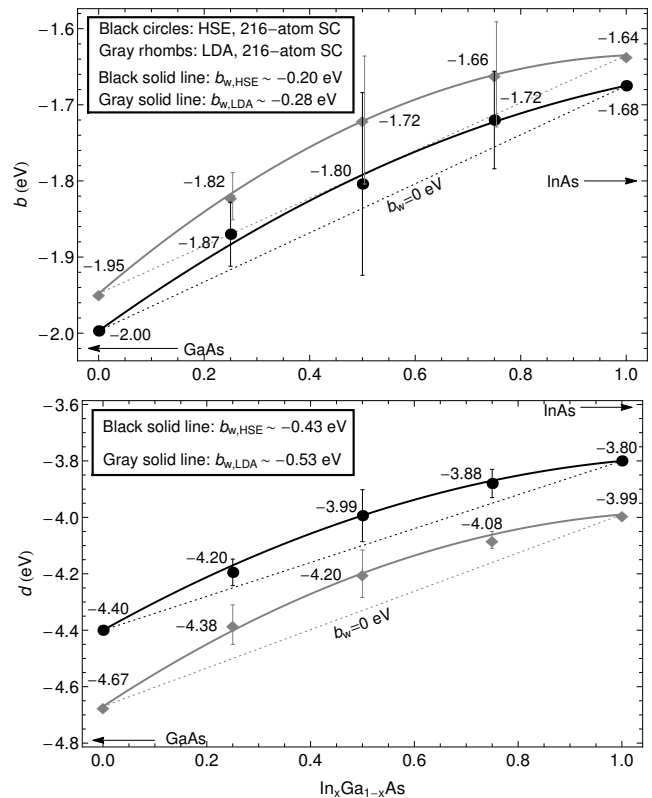


FIG. 3. Compositional dependence of the shear deformation potentials, $D = b$ or d , defined as $D = [D(\epsilon = 0+) + D(\epsilon = 0-)]/2$, where $D(\epsilon = 0+)$ and $D(\epsilon = 0-)$ are calculated for the tensile and compressive strain conditions, using the LDA (gray filled rhombs) and HSE (black filled circles) functionals. All the lines are given by Eq. (1). The recommended values from Ref. 6 are given with arrows. The "error" bars are related to disorder-induced anisotropy, $|D(\epsilon = 0+) - D(\epsilon = 0-)|$.

the difference between the LDA and HSE-calculated b (d) deformation potentials is of $\sim 3\%$ (5%) only. This is likely due the fact that the valence bands are usually well described by the LDA approximation.²³ In Fig. 3, we give some values of b (d) recommended in Ref. 6 for the binary alloys. Our HSE calculations agree well with these recommended data, predicting a somewhat higher (lower) shear deformation potential for InAs (GaAs) by $\sim 10\%$ (0%) and $\sim 5\%$ (8%) for the b and d deformation potentials, respectively. However, we would like to emphasize that there hardly exist reliable experimental data for a proper comparison. The present first-principles study does not rely on any adjustable parameters. It can serve as a reference for future experiments, and can be exploited to test empirical band structure calculations.

Using the first-principles calculations, we can now clarify whether the compositional bowing of shear deformation potentials is strong or not. Figure 3 clearly shows a nonlinear compositional dependence of the b and d parameters. This bowing is not as strong as that pre-

dicted for group-III nitride alloys in Ref. 11, but it reveals the apparent limitation of Vegard's law, which is often assumed for the band energy deformation potentials of ternary alloys.^{6,12} We find that the compositional bowing of the deformation potentials is upward in the $\text{In}_x\text{Ga}_{1-x}\text{As}$ alloys, meaning that the strain dependence for the valence band splitting of ternary alloys with $x \sim 0.5$ is more similar to that of InAs (not GaAs). A plausible explanation for this behavior is that the top valence bands, which show a p -like character, are preferably formed by the p -orbitals of In (not Ga) cation atoms in the $\text{In}_x\text{Ga}_{1-x}\text{As}$ alloys with $x \gtrsim 0.5$. This is confirmed by comparing the relative contribution of In and Ga atomic orbitals to the density of states for the top valence bands. Finally, we notice that there exists some broadening of the b and d parameters because of the disorder-induced anisotropy with respect to the strain parameter sign, see Fig. 3. This broadening of d (b) is, however, weaker than (comparable to) the compositional bowing of d (b). The anisotropy becomes unphysically large for the shear deformation potentials obtained with the 32-atom SQS structures (not reported in Fig. 3) because of a finite-size effect.

In conclusion, we studied the structural, electronic and mechanical properties of strained $\text{In}_x\text{Ga}_{1-x}\text{As}$ ternary al-

loys in a systematic manner, using a first-principles approach for various alloy compositions and strain configurations. The compositional and strain dependencies of the band structure parameters as well as other relevant material parameters (tabulated in SM, see Ref. 22) were obtained for these semiconductor compounds, allowing for device simulations within the framework of the tight-binding and drift-diffusion models. We found that the band energies and their deformation potentials can exhibit a significant compositional bowing. Using the energy and atom-resolved density of states, the role of In cation atoms was revealed in relation to the bowing direction of the InGaAs deformation potentials. That suggested a simple way to understand the bowing effect in semiconductor alloys in a qualitative manner.

ACKNOWLEDGMENTS

This research is funded by the EU Commission (FP7 project: DEEPEN). The computer simulations are done at the Swiss National Supercomputer Center (project: s579).

* petr.k@iis.ee.ethz.ch

- ¹ M. Wu, Y. I. Alivov, and H. Morkoç, *Journal of Materials Science: Materials in Electronics* **19**, 915951 (2008).
- ² A. M. Ionescu and H. Riel, *Nature* **479**, 329337 (2011).
- ³ K. J. Kuhn, *IEEE Transactions on Electron Devices* **59**, 1813 (2012).
- ⁴ F. H. Pollak and M. Cardona, *Physical Review* **172**, 816 (1968).
- ⁵ G. Signorello, E. Lörtscher, P. A. Khomyakov, S. Karg, D. L. Dheeraj, B. Gotsmann, H. Weman, and H. Riel, *Nature Communications* **5**, 3655 (2014).
- ⁶ I. Vurgaftmana, J. R. Meyer, and L. R. Ram-Mohan, *Applied Physics Review* **89**, 5815 (2001).
- ⁷ M. L. Cohen and T. K. Bergstresser, *Physical Review* **141**, 789 (1966).
- ⁸ L. Nordheim, *Annalen der Physik (Leipzig)* **9**, 607 (1931).
- ⁹ P. A. Khomyakov, W. Andreoni, N. D. Afify, and C. Curioni, *Physical Review Letters* **107**, 255502 (2011).
- ¹⁰ L. Bellaiche and D. Vanderbilt, *Physical Review B* **61**, 7877 (2000).
- ¹¹ S. P. Lepkowski, I. Gorczyca, K. Stefańska-Skrobas, N. E. Christensen, and A. Svane, *Physical Review B* **88**, 081202(R) (2013).
- ¹² Q. Yan, P. Rinke, A. Janotti, M. Scheffler, and C. G. Van de Walle, *Physical Review B* **90**, 125118 (2014).
- ¹³ A. Zunger, S. H. Wei, L. G. Ferreira, and J. E. Bernard, *Physical Review Letters* **65**, 353 (1990).
- ¹⁴ C. K. Gan, Y. P. Feng, and D. J. Srolovitz, *Physical Review B* **73**, 235214 (2006).
- ¹⁵ C. J. Wu, J. Zheng, C. L. Zacherl, P. Wu, Z.-K. Liu, and R. Xu, *Journal of Physical Chemistry C* **115**, 19741 (2011).
- ¹⁶ P. E. Blöchl, *Physical Review B* **50**, 17953 (1994).

- ¹⁷ G. Kresse and J. Furthmüller, *Physical Review B* **54**, 11169 (1996).
- ¹⁸ G. Kresse and J. Furthmüller, *Computational Materials Science* **6**, 15 (1996).
- ¹⁹ J. Perdew and A. Zunger, *Physical Review B* **23**, 5048 (1981).
- ²⁰ J. Heyd, G. E. Scuseria, and M. Ernzerhof, *Journal of Chemical Physics* **124**, 219906 (2006).
- ²¹ F. Sökeland, M. Rohlfing, P. Krüger, and J. Pollmann, *Physical Review B* **68**, 075203 (2003).
- ²² See supplementary material at the URL for additional computational details and the tabulated numerical data of the band energies, deformation potentials, lattice parameters and elastic constants as well as their bowing parameters.
- ²³ C. G. Van de Walle, *Physical Review B* **39**, 1871 (1989).
- ²⁴ K. H. Goetz, D. Bimberg, H. Jurgensen, J. Selders, A. V. Solomonov, G. F. Glinskii, and M. Razeghi, *Journal of Applied Physics* **54**, 4543 (1983).
- ²⁵ G. E. Pcus, *Journal of Experimental and Theoretical Physics* **14**, 1075 (1962).

SUPPLEMENTARY MATERIAL

Hybrid functional calculations

To calculate the electronic, structural and mechanical properties of the strained InGaAs compounds, we employ the conventional HSE06 hybrid functional functional with 25% of the short-range Fock exchange and the range-separation parameter of $\mu = 0.207 \text{ \AA}^{-1}$ for all alloy compositions. However, ion relaxation is first done

using the semi-local GGA-PBE functional to have a good initial guess for atomic positions in alloy structures. Subsequently, we perform total energy calculations with the HSE06 functional to achieve a better convergence for the atomic and electronic structure of alloys. Even though this second ion optimization procedure usually affects the HSE-calculated electronic structure marginally, it is particularly important for an accurate calculation of the strain II deformation potential, d . The shear strain II induces an internal strain in the InGaAs alloy structures, giving rise to a piezoelectric effect. Accounting for this effect properly requires calculating the interatomic forces and band energies in a consistent manner, i.e., with the same functional for all the physical quantities.

For a 216-atom supercell, we have found that the band structure energies are sufficiently accurate if a lower kinetic energy cut-off of 300 eV and a Γ -point for the short-range Fock exchange part of a hybrid functional are adopted. That allows reducing the computational burden of hybrid functional calculations without compromising the required accuracy. The induced error (upward shift) is of ~ 20 meV, which is given by the difference between the 32-atom SQS (2-atom primitive cell) and 216-atom supercell-calculated band parameters for the binary alloys as seen in Fig. 1 in the main text and Table SI in supplementary material. This shift is within an acceptable error bar since it is much smaller than the difference between the calculated and experimental values of the band energies.

Lattice parameter definition for ternary alloys

To understand the structural properties of the InGaAs compounds, we have adopted two structural models (the 32-atom SQS and 216-atom cubic supercells) as discussed in the manuscript. In both cases, an effective 2-atom cubic cell is assumed for calculating a lattice parameter, a , of ternary alloys, which is derived from a simple relation between the supercell volume (Ω) and lattice constant (a), $\Omega = N_u a^3$, where N_u is the number of 2-atom cells constituting the SQS or cubic supercell structures. To calculate the lattice parameter, a full structural optimization has been done for the ternary alloy model structures. We have found essentially no compositional bowing of the lattice constant for the fully optimized InGaAs structures, i.e., $b_w \sim 0$. Doing ion relaxation is crucial to account for the effect of alloy disorder in ternary alloys properly. Otherwise, it would lead to the wrong prediction of an upward ($b_w < 0$) compositional bowing for the lattice constant of the InGaAs ternary alloys in spirit of the VCA that does not allow any ion relaxation. Note that the HSE-calculated lattice constant for GaAs (InAs) is just 0.5% (0.8%) larger than the corresponding experimental parameter as seen in Table SI. Thus, the hybrid functional approach can be expected to give the lattice parameters of the InGaAs alloys with a similar accuracy.

Compositional dependence of elastic constants

Another explanation for the apparent discrepancy between the DFT-calculated and experimental values of the band-gap deformation potential is that the measurement for the $\text{In}_x\text{Ga}_{1-x}\text{As}$ alloy with $x = 0.53$ was done under general strain conditions. It means that it requires separating the hydrostatic and shear strain effects on the band-gap energy to determine the actual hydrostatic deformation potential. This separation procedure relies on the knowledge of other alloy material parameters such as elastic constants, which are usually assumed to be given by Vegard's law. However, we have found that the elastic constants of the InGaAs compounds exhibit some downward compositional bowing that might need to be taken into consideration for more accurate interpretation of the experimental data. In Table SI, we report the elastic constants of the binary alloys (GaAs and InAs) as well as the corresponding compositional bowing parameters for the InGaAs ternary alloy calculated with the HSE functional. The table shows that the elastic constants of the binary alloys agree very well (within ~ 1 -2%) with the existing experimental data. A somewhat larger deviation of $\sim 6\%$ is found for $C_{12,\text{GaAs}}$.

Conduction band deformation potentials

We would like to notice that the conduction band hydrostatic deformation potentials, a_Γ , a_L and a_X , in Table SI can be expressed as $a_\Gamma = \Xi_{d,\Gamma} - a_V$ and $a_C = \Xi_{d,C} + \Xi_{u,C}/3 - a_V$, where $C = L$ or X , and $\Xi_{d,\Gamma}$, $\Xi_{d,C}$ and $\Xi_{u,C}$ are the deformation potentials as defined by Herring and Vogt [Phys. Rev. **101**, 944 (1956)], and a_V is the hydrostatic deformation potential for the average of three top valence bands at the Γ point. The electronic states at the Γ and L (Γ and X) valleys of the face-centered cubic BZ are not affected by the shear strain I (II), being protected by symmetry, i.e., $\Xi_{u,\Gamma} = 0$. The three X (four L) valleys are split by the shear strain I (II) into three singlets (doublets) with a shift of $\Delta E_X = 0$ and $\Delta E_X = \pm \Xi_{u,X} |\epsilon|$ ($\Delta E_L = \pm 2 \Xi_{u,L} |\epsilon|/3$) with respect to the averaged conduction band energy. The conduction band deformation potentials are tabulated in Table SII.

VCA vs. supercell calculations of ternary alloys

For the sake of comparison, we have done explicit virtual crystal approximation (VCA) calculations based on density functional theory (DFT), using a version of DFT-VCA proposed by Bellaiche and Vanderbilt [Phys. Rev. B **61**, 7877 (2000)]. In Fig. S1, the obtained results show that this DFT-VCA scheme predicts an anomalous downward compositional bowing of the lattice constant for InGaAs ternary alloys in consistency with findings of Sökeland and co-workers [Phys. Rev. B **68**, 075203 (2003)] for InGaN ternary alloys. It means that the DFT-VCA fails to reproduce the linear compositional dependence (no bowing) of the lattice parameter of InGaAs suggested by experiment and our supercell calculations. Using the DFT-VCA also results in an unphysical downward compositional bowing of the band gap and higher

conduction band energies as seen in Fig. S1. For example, the compositional dependence of the band gap energy has a significant contribution of the third-order correction (x^3) in contradiction with the supercell calculations and experimental data. If we impose no bowing for the lattice parameter in the DFT-VCA calculations (strained VCA), the compositional bowing of the band

gap increases significantly, showing even stronger deviation from the experimental findings and supercell calculations, see Fig. S1. Sökeland and co-workers have proposed that these failures of DFT-VCA are due to rather different lattice constants of alloy components (InN and GaN in their case, and InAs and GaAs in our case) as well as a very different localization of the In and Ga electronic states that are to be mixed in the VCA calculations.

TABLE I. Material parameters of the InGaAs compounds calculated using the HSE06 functional. The conduction band energies of the binary alloys (GaAs and InAs), E_Γ , E_L , E_X , and E_X^* (in eV), as well as the hydrostatic and shear deformation potentials, a_Γ , a_L , a_X , a_X^* , b and d (in eV), are calculated for a 2-atom primitive cell without the spin-orbit coupling included. The spin-orbit splitting, Δ_{so} , given in the table allows accounting for the spin-orbit interaction effect on the band energies within a $k \cdot p$ model. In the parenthesis, we report the conduction band energies obtained with the spin-orbit coupling included; the experimental lattice constants have been adopted in this case. The lattice parameters, a , and elastic constants, C_{11} , C_{12} and C_{44} , are given in units of Å and GPa, respectively. Any material parameter, Q , for a given ternary alloy composition, x , can be obtained using the interpolation formula Eq. (1) in the main text, where the bowing parameters, b_w , are obtained using 216-atom supercell model structures for the InGaAs ternary alloys. The compositional dependence of the band energy, E_X , at the X valley minimum can be approximated as $E_X(x) = x E_{X,\text{InAs}} + (1-x) E_{X,\text{GaAs}}^* - b_w x(1-x)$ for $x > 0.25$. The same approximation can be adopted for a_X . As an example, we give the parameters for the most relevant alloy, $\text{In}_{0.53}\text{Ga}_{0.47}\text{As}$. The experimental data are given at room temperature, Vurgaftmana *et al* [Appl. Phys. Rev. **89**, 5815 (2001)] and K.-H. Goetz *et al* [J. Appl. Phys. **54**, 4543 (1983)].

	E_Γ	E_L	E_X	E_X^*	Δ_{so}	a_Γ	a_L	a_X	a_X^*	b	d	C_{11}	C_{12}	C_{44}	a
GaAs	1.29 (1.32)	1.72 (1.65)	2.05 (1.91)	2.09 (1.95)	0.36 (0.36)	-8.54	-3.35	1.39	1.76	-2.01	-4.33	117.5	50.0	60.3	5.677
Exp	1.42	1.81	1.97	-	0.34	-8.33	-	-	-	-2.0	-4.8	119.0	53.4	59.6	5.653
$\text{In}_{0.53}\text{Ga}_{0.47}\text{As}$	0.66 (0.69)	1.57 (1.51)	2.11 (1.95)	2.11 (1.95)	0.37 (0.37)	-6.81	-2.79	1.50	1.50	-1.79	-3.90	96.5	46.9	45.2	5.891
Exp	0.75	-	-	-	-	-7.79	-	-	-	-	-	-	-	-	5.868
InAs	0.36 (0.39)	1.58 (1.53)	2.17 (2.00)	2.17 (2.00)	0.38 (0.38)	-5.97	-2.69	1.45	1.45	-1.69	-3.72	85.2	45.2	40.3	6.104
Exp	0.35	-	-	-	0.39	-6.08	-	-	-	-1.8	-3.6	83.4	45.4	39.5	6.058
b_w	0.55	0.31	-	0.105	0	-1.47	-0.83	-	0.40	-0.20	-0.43	15.5	2.2	17.9	~ 0
Exp	0.48	-	-	-	-	2.34	-	-	-	-	-	-	-	-	~ 0

TABLE II. Hydrostatic and shear deformation potentials of the InGaAs compounds calculated using the HSE06 functional for the conduction band valleys, $\Xi_{d,\Gamma} - a_V$, $\Xi_{d,X} - a_V$, $\Xi_{u,X}$, $\Xi_{d,L} - a_V$ and $\Xi_{u,L}$ in units of eV, where a_V is the hydrostatic deformation potential for the average of three top valence bands at the Γ point. We note that $\Xi_{u,\Gamma} = 0$. The experimental data are taken from *Landolt-Börnstein, Numerical Data and Functional Relationships in Science and Technology* (Springer, New York, 1982), Group III, Vol. 17a-b. In the parenthesis and last column, we give the theoretical values of deformation potentials, Ξ_u^{LDA} and a_V^{LDA} , which were obtained using the DFT-LDA calculations for the binary alloys (GaAs and InAs) by Chris Van de Walle [Phys. Rev. B **39**, 1871 (1989)], and Vegard's law is used to estimate the value of a_V for the $\text{In}_{0.53}\text{Ga}_{0.47}\text{As}$ alloy. The compositional dependence of the deformation potential, $\Xi_{u,X}$, can be approximated as $\Xi_{u,X}(x) = x \Xi_{u,X,\text{InAs}} + (1-x) \Xi_{u,X,\text{GaAs}}^* - b_w x(1-x)$ for $x > 0.25$.

	$\Xi_{d,\Gamma} - a_V$	$\Xi_{d,X} - a_V$	$\Xi_{u,X}$	$\Xi_{d,X}^* - a_V$	$\Xi_{u,X}^*$	$\Xi_{d,L} - a_V$	$\Xi_{u,L}$	$\Xi_{u,L}^{\text{exp}}$	a_V^{LDA}
GaAs	-8.54	-1.35	8.22 (8.61)	-0.34	6.30	-8.38	15.1 (14.26)	19.6	1.16
$\text{In}_{0.53}\text{Ga}_{0.47}\text{As}$	-6.81	-0.22	5.15	-0.22	5.15	-7.09	12.9	-	1.08
InAs	-5.97	-0.16	4.83 (4.50)	-0.16	4.83	-6.86	12.5 (11.35)	-	1.00
b_w	-1.47	-	-	-0.10	1.50	-1.96	3.38	-	-

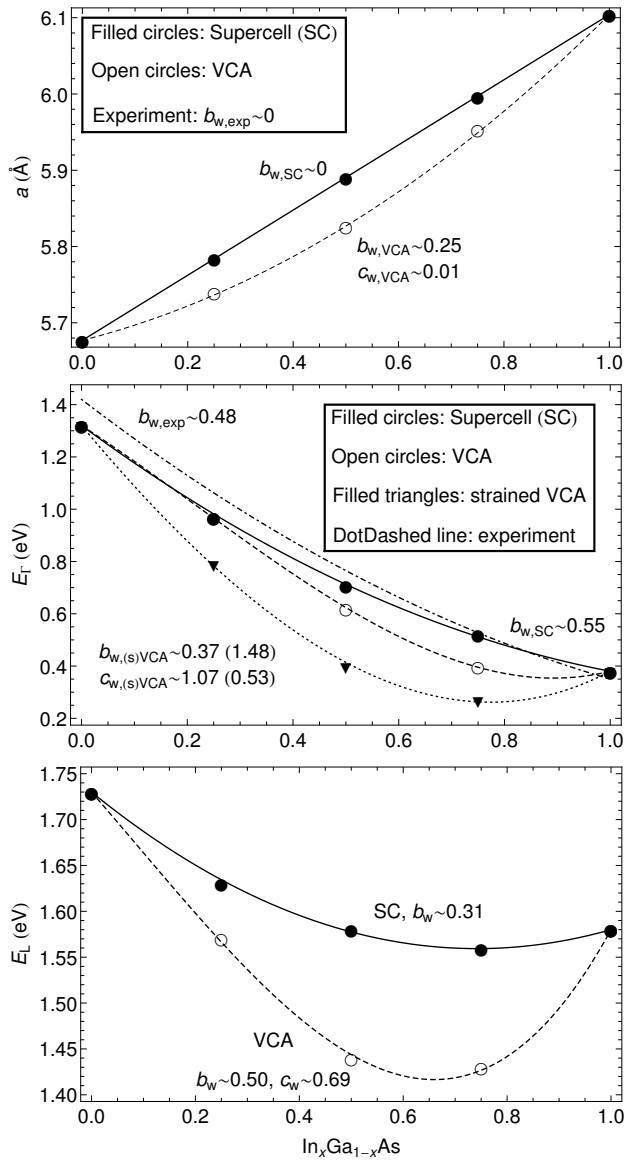


FIG. 4. Compositional dependence of the lattice constant, a (top), band gap energy (middle), and L -valley conduction band energy (bottom) calculated using the HSE functional for two alloy models based on (i) 216-atom supercell (SC), and (ii) 2-atom virtual crystal approximation (VCA) by Bellaiche and Vanderbilt. Filled (open) black circles correspond to supercell (VCA) calculations. Filled black triangles correspond to strained VCA calculations where the supercell-calculated lattice constant is adopted, i.e., assuming no bowing for the lattice constant. The solid and dotdashed black lines are given by the formula Eq. (1), and the dashed and dotted black lines are given by a modified formula Eq. (1) where a third-order term, $-c_w x^2(1-x)$, is added for having a better fit of VCA data points. In parenthesis, we give bowing parameters for strained VCA.